Pergamon

Geochimica et Cosmochimica Acta, Vol. 67, No. 17, pp. 3201–3214, 2003

0016-7037/03 $30.00 + .00

doi:10.1016/S0016-7037(03)00083-8

Barium isotopes in individual presolar silicon carbide grains from the Murchison meteorite

MICHAEL R. SAVINA,[1,*] ANDREW M. DAVIS,[2,3] C. EMIL TRIPA,[1,2] MICHAEL J. PELLIN,[1] ROBERT N. CLAYTON,[2,3,4] ROY S. LEWIS,[2] SACHIKO AMARI,[5] ROBERTO GALLINO,[6] and MARIA LUGARO[7]

[1]Materials Science Division, Argonne National Laboratory, Argonne, IL 60439, USA
[2]Enrico Fermi Institute,
[3]Department of the Geophysical Sciences and
[4]Department of Chemistry, University of Chicago, Chicago, IL 60637, USA
[5]Laboratory for Space Sciences, Washington University, St. Louis, MO 63130, USA
[6]Dipartimento di Fisica Generale, Università di Torino and Sezione INFN di Torino, I-10125 Torino, Italy
[7]Institute of Astronomy, Cambridge University, Madingley Road, Cambridge CB3 0HA, United Kingdom

(*Received April* 10, 2002; *accepted in revised form December* 11, 2002)

Abstract—Barium isotopic compositions of single 2.3–5.3 μm presolar SiC grains from the Murchison meteorite were measured by resonant ionization mass spectrometry. Mainstream SiC grains are enriched in *s*-process barium and show a spread in isotopic composition from solar to dominantly *s*-process. In the relatively coarse grain size fraction analyzed, there are large grain-to-grain variations of barium isotopic composition. Comparison of single grain data with models of nucleosynthesis in asymptotic giant branch (AGB) stars indicates that the grains most likely come from low mass carbon-rich AGB stars (1.5 to 3 solar masses) of about solar metallicity and with approximately solar initial proportions of *r*- and *s*-process isotopes. Measurements of single grains imply a wide variety of neutron-to-seed ratios, in agreement with previous measurements of strontium, zirconium and molybdenum isotopic compositions of single presolar SiC grains. *Copyright © 2003 Elsevier Ltd*

1. INTRODUCTION

Pristine interstellar grains that predate the formation of the solar system were first isolated from meteorites fifteen years ago (Lewis et al., 1987). A number of different minerals have been identified as presolar, including diamond (Lewis et al., 1987), SiC (Bernatowicz et al., 1987; Tang and Anders, 1988), graphite (Amari et al., 1990), corundum (Hutcheon et al., 1994; Nittler et al., 1994), Si_3N_4 (Nittler et al., 1995), spinel (Choi et al., 1998), and hibonite (Choi et al., 1999). In addition, presolar silicates have been discovered in interplanetary dust particles (Messenger et al., 2002). All types except diamond occur as grains that are large enough to be analyzed individually. Their identification as presolar grains rests on isotopic compositions of major and minor elements, which are so anomalous compared to solar composition that they must be of nuclear, not chemical, origin. These large isotope anomalies also require that presolar grains escaped homogenizing processes that took place during the formation of the solar system. Each grain samples ejecta from a single star and records evidence of nucleosynthetic processes in that star and those that contributed to the initial composition of that star. The best-studied presolar grains to date are SiC, largely because they are relatively abundant compared to other kinds of presolar grains and contain a number of elements of nucleosynthetic interest.

The isotopic compositions of major elements in presolar SiC grains have been well characterized, and this has led to a classification based on carbon, nitrogen, and silicon isotopic compositions (e.g., Zinner, 1998). Ion microprobe studies have shown that ~90% of SiC grains belong to the mainstream type, the main features of which are $^{12}C/^{13}C$ ratios between 20 and 100, and enhancements in $^{14}N/^{15}N$, $^{29}Si/^{28}Si$ and $^{30}Si/^{28}Si$ compared to solar system ratios. Mainstream SiC grains are believed to have condensed in the mass-losing envelopes of carbon-rich low mass (~1.5 to ~5 $M_\odot$) thermally pulsing asymptotic giant branch (TP-AGB) stars. Many of these stars are known to show SiC emission lines from circumstellar dust (Treffers and Cohen, 1974; Olnon et al., 1986; Volk et al., 1991) and to be enriched in the products of *s*-process nucleosynthesis, in which neutron capture occurs at a rate slow enough for unstable nuclei to decay before capturing another neutron (Burbidge et al., 1957; Clayton, 1968; Wallerstein et al., 1997). See Wallerstein and Knapp (1998) for a review of carbon stars.

The AGB is the most advanced nuclear-burning phase of normal stellar evolution of low- to intermediate-mass stars (up to ~8 $M_\odot$), in which the extended envelope is progressively lost by efficient stellar winds, leaving an electron-degenerate carbon-oxygen core as a white dwarf (Iben and Renzini, 1983; Lattanzio and Boothroyd, 1997; Straniero et al., 1997; Mowlavi, 1999; Goriely and Mowlavi, 2000; Herwig, 2000). By the time a star has reached the AGB, it has a carbon-oxygen core and a hydrogen-rich envelope, between which is a helium- and carbon-rich region referred to as the helium intershell. Most of the time, hydrogen burning occurs in a shell at the base of the envelope, producing a growing region of nearly pure helium. This newly formed helium sinks, increasing the mass, density and temperature of the helium intershell until helium begins burning to ^{12}C at the base, causing a thermal runaway (Schwarzschild and Härm, 1965). This thermal instability causes the helium intershell to become convective (developing a pulse-driven convective zone) for a few tens to a few hundred years, and mixing newly formed ^{12}C and *s*-process products throughout the helium intershell. The large amount of energy released in the thermal runaway causes the entire star to expand and

* Author to whom correspondence should be addressed (msavina@anl.gov).

cool, turning off hydrogen-burning at the base of the envelope. Shortly after the quenching of the thermal pulse, the hydrogen-rich convective envelope of the star may extend into the helium intershell, dredging up newly synthesized material, including helium, ^{12}C and *s*-process products, in a so-called "third dredge-up" (TDU) event. Although the ability of stellar models to produce third dredge-up is debated (Frost and Lattanzio, 1996; Straniero et al., 1997; Mowlavi, 1999; Herwig, 2000), there is no question that it occurs in nature. The entire cycle of hydrogen-burning, thermal pulsing and third dredge-up occurs recurrently, with interpulse periods of a few thousand to a few tens of thousands of years. With successive third dredge-up events, the initially oxygen-rich envelope (C/O<1) becomes progressively enriched in carbon and may eventually become carbon-rich (C/O>1). It is generally believed that in intermediate-mass stars (M > ~5 to ~8 $M_\odot$), proton captures on carbon at the bottom of the convective envelope (hot bottom burning) prevent the stellar envelope from becoming carbon-rich (Boothroyd et al., 1993).

In low-mass AGB stars, *s*-process nucleosynthesis occurs in the helium intershell (see section 4.1 for more details on how this occurs), and the products are mixed into the envelope during third dredge-up events. Stellar winds drive mass loss from the envelope. Oxide and silicate grains may condense in these outflows early in the AGB phase when the envelope is oxygen-rich. SiC grains with *s*-process enhancements condense in stellar outflows during the later stages of the AGB when the envelope is carbon-rich (Lodders and Fegley, 1995; Sharp and Wasserburg, 1995). For a more detailed discussion of the AGB phase and *s*-process nucleosynthesis see, for example, Busso et al. (1999).

Measurements of isotopic compositions of heavy trace elements in bulk samples (aggregates of many grains) of presolar SiC grains have shown enhancements in the *s*-process isotopes of the noble gases xenon (Srinivasan and Anders, 1978; Lewis et al., 1990, 1994) and krypton (Alaerts et al., 1980; Ott et al., 1988; Lewis et al., 1990, 1994), as well as barium (Ott and Begemann, 1990a,b; Zinner et al., 1991; Prombo et al., 1993), strontium (Ott and Begemann, 1990b; Richter et al., 1992), neodymium (Zinner et al., 1991; Richter et al., 1992, 1993), samarium (Zinner et al., 1991; Richter et al., 1992, 1993), and dysprosium (Richter et al., 1994a,b).

Previous studies of individual presolar SiC grains have shown that most are enhanced in the *s*-process isotopes of zirconium (Nicolussi et al., 1997a; Davis et al., 1998), molybdenum (Nicolussi et al., 1998a; Davis et al., 1999) and strontium (Nicolussi et al., 1998b), but that the degree of *s*-process enhancement can vary widely from grain to grain. These studies and the work of Gallino et al. (1997) on the interpretation of isotopic data for heavy elements in aggregates of presolar grains strongly suggest that most presolar SiC grains form in mass-losing envelopes of TP-AGB stars, and that: (1) the parent AGB stars were initially of near-solar isotopic composition and near-solar metallicity; (2) the grains came from many AGB stars with a wide range of neutron/seed ratios, since a particular AGB stellar model with one choice of parameters is only capable of producing a narrow range of isotopic composition; and (3) the grains must come from AGB stars of low mass, ~1.5 to ~3 $M_\odot$ (Davis et al., 2001; Lugaro et al., 2003).

Our prior studies of heavy elements in single grains focused on the first peak in the solar *s*-process abundance curve vs. atomic mass at the neutron magic number N = 50. This paper describes new measurements of the isotopic composition of barium, the most abundant element in the second peak at the next neutron magic number (N = 82), in single presolar grains. Barium has seven stable isotopes. In Figure 1, the main *s*-process path in the Ba region, which consists of neutron captures and β^- decays, is indicated by a heavy line. Branchings that can be activated under conditions of higher neutron density or temperature are indicated by lighter lines. The branches at unstable cesium isotopes are particularly important. Overall, barium is an *s*-process element: ~80% of its abundance in the solar system derives from the *s*-process in AGB stars (Käppeler et al., 1989; Arlandini et al., 1999; Travaglio et al., 1999). ^{130}Ba and ^{132}Ba are produced by the *p*-process and are of very low abundance; ^{134}Ba and ^{136}Ba are exclusively *s*-process isotopes; neutron magic ^{138}Ba is mostly of *s*-process origin; and the odd isotopes ^{135}Ba and ^{137}Ba are of mixed *r*- and *s*-process contribution. While most of solar ^{135}Ba is produced by the *r*-process (74%), ^{137}Ba has a low neutron capture cross section and 65% of solar ^{137}Ba is of *s*-process origin (Arlandini et al., 1999; Travaglio et al., 1999).

Previous studies of barium isotopes in presolar grains used Thermal Ionization Mass Spectrometry (TIMS) and Secondary Ion Mass Spectrometry (SIMS) to measure isotopic compositions of aggregate samples containing large numbers of μm and sub-μm grains segregated by size, and found large enhancements of the *s*-only isotopes ^{134}Ba and ^{136}Ba compared to all other barium isotopes (Ott and Begemann, 1990a,b; Zinner et al., 1991; Prombo et al., 1993). Ott and Begemann (1990a) measured two aggregate SiC samples from a Murchison acid-resistant residue and extrapolated from solar isotopic composition through their measured data to calculate the isotopic composition of a pure *s*-process component. This extrapolation was possible since they were able to measure the abundances of the *p*-only isotopes ^{130}Ba and ^{132}Ba. Indeed any *p*-only isotope is bypassed by the main *s*-process flow and its initial abundance in the *s*-process region is destroyed by neutron captures. Since the ratio of neutron magic ^{138}Ba to *s*-only ^{136}Ba is sensitive to the mean neutron exposure, the extrapolated pure *s*-process component compositions (which corresponds to $\delta^{138}Ba = -290 \pm 64‰$) led Ott and Begemann to conclude that the total neutron exposure needed to explain this component was about half that needed to explain the solar system *s*-process component (which corresponds to $\delta^{138}Ba = -138 \pm 30‰$). They also found a nonsolar $^{134}Ba/^{136}Ba$ ratio, but could not show that it was not due to instrumental mass fractionation; some later work hinted that the nonsolar $^{134}Ba/^{136}Ba$ ratio was characteristic of presolar SiC (Ott and Begemann, 1990b). Zinner et al. (1991) measured size-separated SiC aggregates by SIMS in the Murchison KJ-series separates (Amari et al., 1994) and found a correlation between grain size and isotopic composition. Although they did not measure *p*-only ^{130}Ba and ^{132}Ba, the correlations were consistent with mixing between an *s*-component and normal solar isotopic composition. They were able to show that the grains have a nonsolar $^{134}Ba/^{136}Ba$ ratio, despite the fact that both ^{134}Ba and ^{136}Ba are *s*-only isotopes, which provided an additional indication that the grains sampled an *s*-process component that differed from that of the solar system.

Prombo et al. (1993) measured all seven barium isotopes

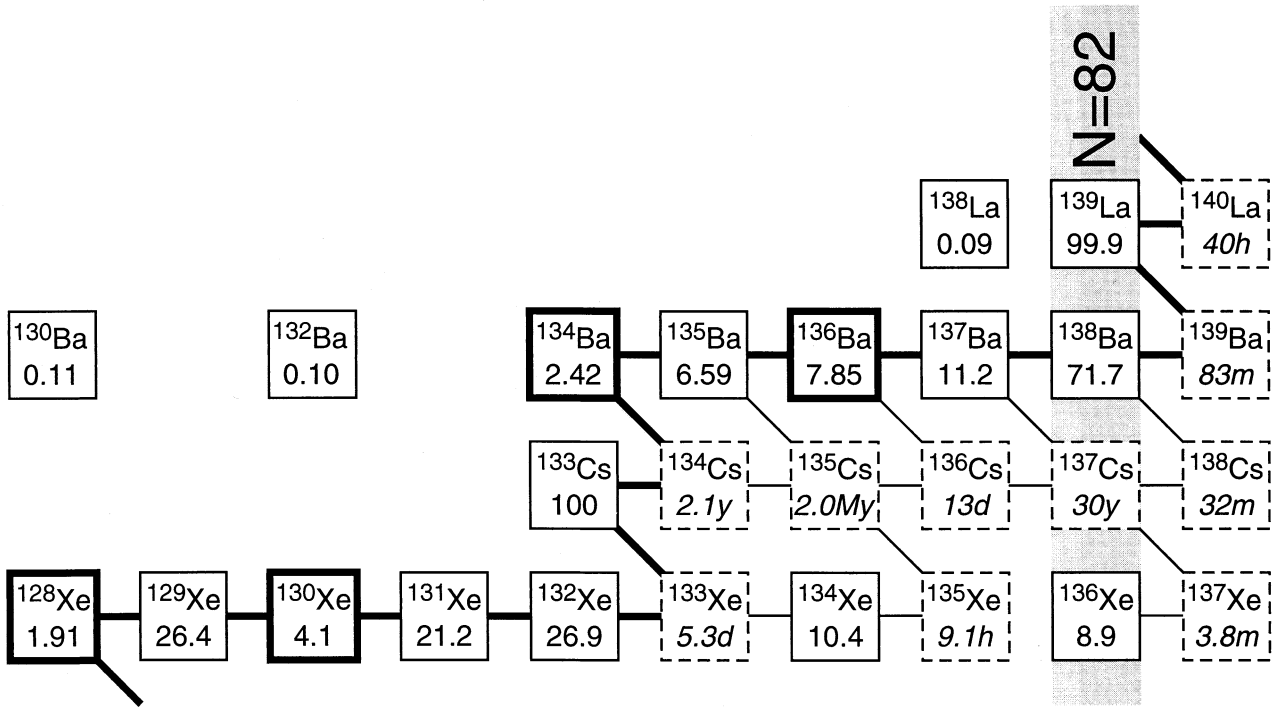

Fig. 1. Barium region of the chart of the nuclides. Percent abundances (nonitalic) are shown for each stable isotope and laboratory half-lives (italic) for each unstable isotope (half-lives at stellar temperatures may be different, as discussed in the text). The main *s*-process path is shown as a bold line and branches along the *s*-path are shown as finer lines; *s*-only isotopes are outlined in bold lines.

with high precision in some of the same grain size separates as Zinner et al. (1991). They were able to decompose their barium isotopic compositions into a pure *s*-process component (the "G-component"), and a component of solar system isotopic composition (the "*N*-component"), which they assumed to represent an initial stellar atmosphere component. Both Zinner et al. (1991) and Prombo et al. (1993) were able to show that a spread of G-components vs. grain size exists ($\delta^{138}Ba_G$ ranges from -260 ± 85 to -397 ± 65‰), with decreasing values (lower mean neutron exposures) inferred for increasing grain size. Gallino et al. (1993) compared all of the aggregate data with models of nucleosynthesis in low-mass AGB stars. These models were sufficiently robust that the discrepancy between models and grain data led these authors to suggest that the best neutron capture cross sections for ^{134}Ba, ^{135}Ba, and ^{137}Ba available at that time, from Beer et al. (1992), were incorrect. This suggestion was confirmed in precise measurements by Voss et al. (1994), whose Maxwellian average cross sections of ^{135}Ba and ^{137}Ba are a factor of two higher than those of Beer et al., but some additional recent measurements by Koehler et al. (1998) have brought back a 20% discrepancy in the cross section for ^{137}Ba (Lugaro et al., 2003).

The long-lived isotope ^{135}Cs ($T_{1/2}$ = 2.3 Ma) accumulates during the thermal pulsing phase of AGB stars. Lugaro et al. (2002) compared the linear correlation between ^{135}Ba/^{136}Ba and ^{130}Ba/^{136}Ba in the TIMS data (Ott and Begemann, 1990a; Prombo et al., 1993) with calculated isotopic compositions for AGB stars to show that there is no contribution to ^{135}Ba from decay of ^{135}Cs after grain formation, which is consistent with the timescale of AGB star evolution.

In this paper, we report barium isotopic compositions of single presolar SiC grains of the dominant mainstream type. For the first time, we report major element (carbon, nitrogen, and silicon) isotopic compositions on the same grains for which heavy element isotopic compositions were measured. The new data confirm the conclusions reached from earlier studies on strontium, zirconium, and molybdenum isotopes in single grains, and we show here how the new data further constrain parameters in models of *s*-process nucleosynthesis in TP-AGB stars.

2. EXPERIMENTAL

The silicon carbide grains were separated from the Murchison meteorite as described by Amari et al. (1994). In brief, an interior sample of the meteorite was disaggregated and subjected to a series of chemical dissolution steps to remove silicates, metals, sulfides, and organic matter, and separated by density into a variety of fractions containing diamond, graphite, and silicon carbide. The SiC was further separated by grain size. The grains studied in this work are from the size fraction KJG (~6% by mass of the parent KJ SiC separate), with diameters ranging from 2 to 5 μm, and having an average grain diameter of 3.02 μm (Amari et al., 1994). An aliquot of ~1400 grains of KJG was pressed onto a thin sheet of gold attached to a scanning electron microscope mount. The grains on this mount, CHRL 108, were mapped for silicon isotopic composition by ion imaging on the Washington University Cameca ims-3f SIMS (Amari et al., 1999). Most were identified as mainstream, although 11 X-grains (Pellin et al., 1999, 2000a), one Z-grain (Pellin et al., 2000b) and a unique grain with extremely high ^{29}Si/^{28}Si and ^{30}Si/^{28}Si (Amari et al., 1999) were also found. All of the rarer types of grains were analyzed by SIMS at

Table 1. Carbon, nitrogen, silicon and barium isotopic compositions of single presolar SiC grains in Murchison grain size fraction KJG. Uncertainties are $\pm 2\sigma$, calculated from counting statistics as explained in the text. Barium isotopic compositions are normalized to ^{136}Ba; δ^{x}Ba is defined in the text.

Name	Diam. (μm)	^{12}C/^{13}C	^{14}N/^{15}N	δ^{29}Si (‰)	δ^{30}Si (‰)	δ^{135}Ba (‰)	δ^{137}Ba (‰)	δ^{138}Ba (‰)
031-1	3.6	59.7 ± 0.7	2136 ± 231	0 ± 7	13 ± 11	−179 ± 171	−135 ± 127	57 ± 120
053-1	3.3	56.3 ± 0.8	555 ± 91	40 ± 7	42 ± 11	−272 ± 476	−214 ± 226	−232 ± 170
053-5	2.8	50.3 ± 1.0	646 ± 136	144 ± 8	108 ± 12	73 ± 97	33 ± 70	−147 ± 47
061-3	3.3	64.6 ± 1.1	1215 ± 187	60 ± 6	67 ± 11	334 ± 993	−50 ± 677	−185 ± 466
070-1	—	—	—	—	—	−552 ± 111	−334 ± 122	−293 ± 96
089-2	5.3	27.4 ± 0.3	1577 ± 148	88 ± 6	98 ± 11	−107 ± 90	−112 ± 68	−168 ± 51
090-5	4.0	54.2 ± 0.8	3702 ± 321	114 ± 6	91 ± 11	−713 ± 33	−431 ± 39	−284 ± 35
113-1	3.3	57.7 ± 0.8	435 ± 90	73 ± 6	56 ± 11	−723 ± 434	−672 ± 395	−705 ± 232
153-1	3.0	21.7 ± 0.3	5370 ± 1021	90 ± 10	76 ± 13	−408 ± 76	−343 ± 67	−201 ± 60
166-2	3.4	52.9 ± 0.8	1765 ± 476	27 ± 8	58 ± 12	37 ± 158	166 ± 142	83 ± 109
323-1	—	49.1 ± 0.8	2176 ± 492	14 ± 11	13 ± 14	−127 ± 130	−132 ± 104	−62 ± 88
326-1	2.8	41.7 ± 0.7	3479 ± 766	51 ± 10	59 ± 13	−264 ± 110	−256 ± 87	−232 ± 68
327-2	3.7	51.0 ± 0.7	387 ± 38	187 ± 10	127 ± 13	−427 ± 62	−210 ± 51	−257 ± 37
327-4	2.3	50.1 ± 1.0	2160 ± 475	132 ± 12	109 ± 15	−72 ± 194	−89 ± 142	−34 ± 118
342-4	2.7	63.2 ± 1.5	1473 ± 470	41 ± 11	31 ± 14	−275 ± 137	−74 ± 107	−141 ± 79

Washington University for carbon, nitrogen, and silicon isotopic composition, as were ~50 mainstream grains. The mount was then imaged with a scanning electron microscope and the mineralogy of all grains was determined by energy dispersive X-ray analysis. We have previously analyzed some of the SiC grains on this mount for zirconium, molybdenum, strontium, and barium (Pellin et al., 1999, 2000a,b, 2001). We report here the barium isotopic compositions of mainstream grains; isotopic compositions of minor types of grains will be reported elsewhere.

Barium isotopic compositions were measured by Resonant Ionization Mass Spectrometry (RIMS) on the CHARISMA instrument at Argonne National Laboratory, which has been previously described in detail elsewhere (Ma et al., 1995; Nicolussi et al., 1997b). A description of the most recent version of the instrument, along with a detailed procedure for the barium analysis, is given in a companion article in this issue (Savina et al., 2003). All data were normalized to the barium isotopic composition of $BaTiO_3$ powder, which was measured daily and assumed to have normal terrestrial barium isotopic composition as given by Lewis et al. (1983) and reproduced in Table 1 of the companion article. The only significant reported variations in terrestrial barium isotopic composition are from the Oklo natural reactor (Hidaka et al., 1993). A total of 19 presolar SiC grains were analyzed, of which 15 had sufficient barium to permit isotopic analysis.

Barium isotopic analysis was complicated by the fact that the SiC grain mount had been previously mapped for silicon isotopes, and most of the grains we studied were spot-analyzed for carbon, nitrogen, and silicon by SIMS, all using a Cs^+ primary ion beam. This left a considerable amount of implanted ^{133}Cs in the grains, which interfered with the ^{134}Ba and, to a lesser extent, ^{135}Ba peaks. Figure 2 illustrates the difficulty in extracting the ^{134}Ba peak from the ^{133}Cs interference. The region near ^{135}Ba is little affected and the baseline correction is straightforward: an exponential function is fit to the tail of the ^{133}Cs peak on either side of the $m/z = 135$ peak and subtracted from the spectrum. The same method was used for the $m/z = 134$ peak, but the tail of the ^{133}Cs peak here is too large and noisy to permit an accurate baseline correction and obtain meaningful ^{134}Ba/^{136}Ba ratios. The uncertainty in the measurement after baseline correction (expressed in ^{136}Ba-normalized δ values) is given by:

$$2\sigma = 2(\delta+1000)\sqrt{\frac{(^{x}\mathrm{Ba}_{\mathrm{grain}} + \mathrm{N}_{\mathrm{b}})}{(^{x}\mathrm{Ba}_{\mathrm{grain}} - \mathrm{N}_{\mathrm{b}})^2} + \frac{1}{^{136}\mathrm{Ba}_{\mathrm{grain}}} + \frac{1}{^{x}\mathrm{Ba}_{\mathrm{std}}} + \frac{1}{^{136}\mathrm{Ba}_{\mathrm{std}}}}, \quad (1)$$

where N_b is the number of baseline counts subtracted from the peak, and $^{x}Ba_{grain}$, etc. are the number of atoms counted.

Barium is present in decreasing concentration in SiC grains of increasing average size. While there are no concentration measurements for KJG, about half of the single grains in size fraction KJH, the next coarser fraction, contain less than 15 ppm Ba by weight (Amari et al., 1995; Savina et al., 2003). Therefore, it is difficult to analyze a virgin grain for barium and yet leave enough of the grain for carbon, nitrogen, and silicon isotopic analysis by the usual SIMS microprobe method, although there has been some recent success in doing so with presolar SiC from the Indarch EH4 chondrite (Jennings et al., 2002).

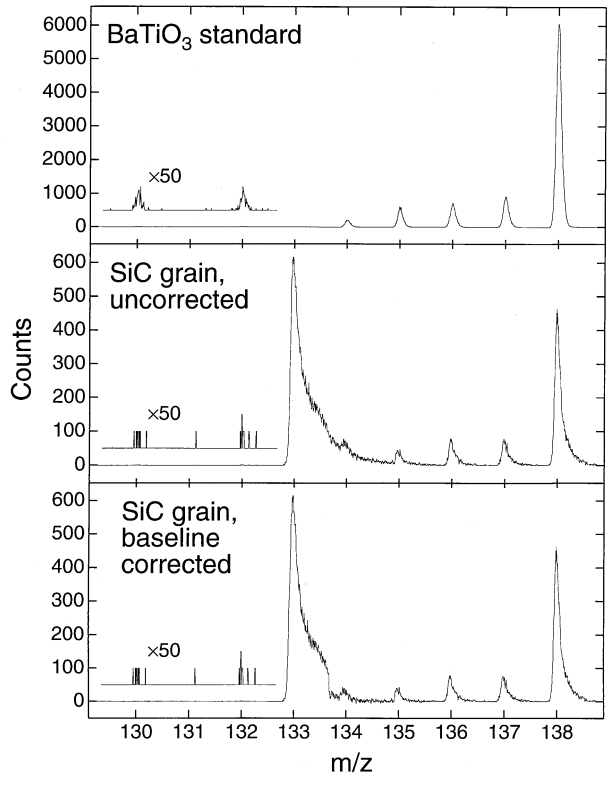

Fig. 2. Barium resonant ionization time-of-flight mass spectra of a terrestrial $BaTiO_3$ standard, mainstream presolar SiC grain 327-2, uncorrected, and mainstream presolar SiC grain 327-2, baseline-corrected in the $m/z = 135$ region. The large peak at m/z 133 is due to nonresonant ionization of cesium implanted during previous SIMS analyses.

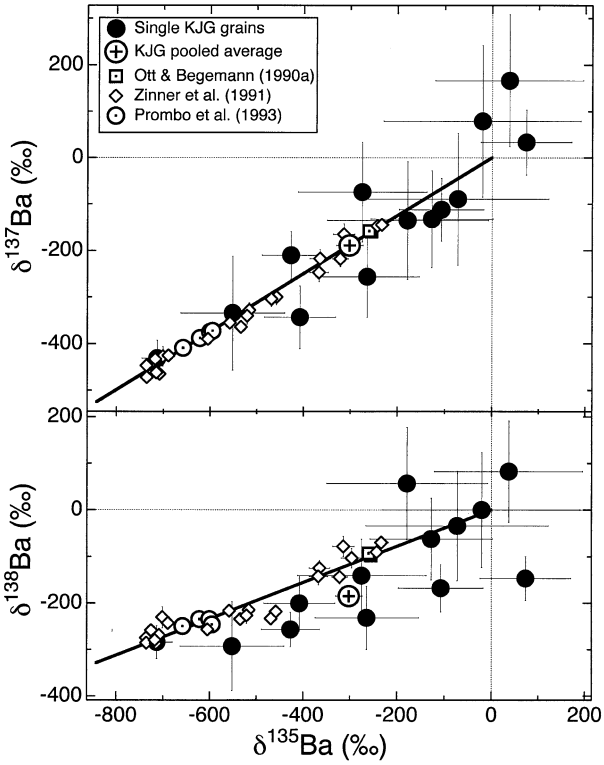

Fig. 3. δ^{137}Ba and δ^{138}Ba vs. δ^{135}Ba, comparing single presolar SiC grains and aggregates of presolar grains. Uncertainties are $\pm 2\sigma$. Grains with uncertainties larger than 300‰ for δ^{135}Ba are not plotted. Gray lines connect the G- and *N*-components calculated by Prombo et al. (1993) for aggregate KJ. Dashed lines connecting these components for aggregates KJA to KJF of Zinner et al. (1991) and KJG (this work) are also plotted, with thicknesses increasing from KJA to KJG.

Presolar SiC grain classification requires isotopic analysis, since the various kinds of presolar SiC grains cannot be distinguished on the basis of morphology or concentrations of minor elements measurable by electron microprobe. A method of determining silicon and carbon isotopes in these grains without using Cs^+ ion bombardment would therefore be valuable.

3. RESULTS

The δ values for ^{135}Ba through ^{138}Ba for each grain are given in Table 1, and are plotted against one another and compared with literature data on presolar SiC aggregates in Figures 3 and 4. We have not plotted data for three grains for which 2σ uncertainties in δ^{135}Ba exceed 300‰. In addition to the single grain data, an average for all grains is given in Table 2 and plotted in these figures for comparison with grain aggregate studies. To obtain the average, the uncorrected spectra were summed and the summed spectrum was baseline-corrected to give a final spectrum. (This is equivalent to measuring all the grains at once.) Table 1 shows that nearly all the grains studied exhibit the *s*-process signature: ^{136}Ba is enhanced relative to ^{135}Ba, ^{137}Ba, and ^{138}Ba. This effect is expressed as negative δ^{135}Ba, δ^{137}Ba, and δ^{138}Ba values. Such *s*-process enhancements were found in previous TIMS and SIMS studies on aggregates of many SiC grains (Ott and Begemann, 1990a; Zinner et al., 1991; Prombo et al., 1993).

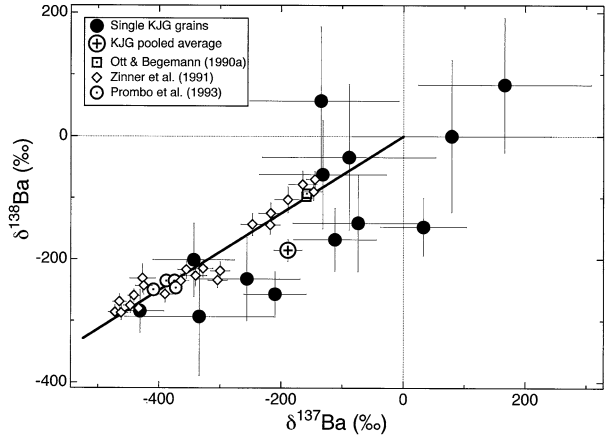

Fig. 4. δ^{138}Ba vs. δ^{137}Ba, comparing single presolar SiC grains and aggregates of presolar grains. Uncertainties are $\pm 2\sigma$. Grains with uncertainties larger than 300‰ for δ^{135}Ba are not plotted. A gray line connects the G- and *N*-components calculated by Prombo et al. (1993) for aggregate KJ. Dashed lines connecting these components for aggregates KJA to KJF of Zinner et al. (1991) and KJG (this work) are also plotted, with thicknesses increasing from KJA to KJG. See Figure 3 for legend.

When δ values are plotted against one another, the aggregate data of Ott and Begemann (1990a), Zinner et al. (1991), and Prombo et al. (1993) lie approximately along straight lines that pass through solar isotopic composition (δ^{x}Ba = 0‰). Solid gray lines connecting the G- and *N*-components calculated by Prombo et al. (1993) for the KJ aggregate, the parent of the size fractions analyzed by Zinner et al. (1991), Prombo et al. (1993), and us, are plotted in Figures 3 and 4. The single grain data group along these lines, as does the KJG average (Figs. 3 and 4). In comparing our data for single grains with literature data for aggregates of grains, there is a tendency for the single grains to lie below the KJ line on plots of δ^{138}Ba vs. δ^{135}Ba and δ^{138}Ba vs. δ^{137}Ba (Figs. 3 and 4); this is more apparent for the pooled average composition. An incorrect ^{133}Cs background correction for ^{135}Ba would cause single grain analyses to deviate from the literature data on δ^{137}Ba vs. δ^{135}Ba and δ^{138}Ba vs. δ^{135}Ba plots (Fig. 3) in the same way, but, since there is no background correction for ^{137}Ba and ^{138}Ba, the δ^{138}Ba vs. δ^{137}Ba plot (Fig. 4) is not affected. Thus, the ^{135}Ba background correction procedure does not appear to be the cause of the discrepancy. The simplest explanation is that there is a deficit in ^{138}Ba in the KJG grains we analyzed.

Zinner et al. (1991) noted that their grain size separates do not lie along a single straight line on a plot of δ^{138}Ba vs. δ^{135}Ba, and that aggregate data for coarser grain size fractions lie increasingly below a line passing through the KJA, KJB and KJC data points and the origin. Our KJG average continues this trend. Following Prombo et al. (1993), we have calculated the G-component compositions of all literature data and our KJG average assuming an *N*-component of normal solar system barium isotopic composition and that the G-component for each size fraction has the δ^{135}Ba value of the G-component in KJ, −839‰. The results are shown in Table 2 and indicate that the G-component for δ^{137}Ba remains constant at approximately −520‰, but for δ^{138}Ba there is a clear decrease with increasing grain size. In Figures 3 and 4, we have plotted lines

Table 2. Barium isotopic composition calculated from the summed counts for all individual grain mass spectra, compared with previous measurements on aggregate samples. Barium isotopic compositions are normalized to ^{136}Ba; δ^{x}Ba is defined in the text.

	Average grain size (μm)[a]	δ^{135}Ba	δ^{137}Ba	δ^{138}Ba	δ^{137}Ba	δ^{138}Ba
		Measured			G-component[b]	
KJG[c]	3.59[d]	−302 ± 24	−189 ± 23	−185 ± 18	−525 ± 76	−514 ± 65
KJF[e]	1.86	−496 ± 40	−327 ± 31	−229 ± 7	−554 ± 67	−387 ± 32
KJE[e]	1.14	−560 ± 51	−358 ± 36	−230 ± 27	−536 ± 73	−344 ± 52
KJD[e]	0.81	−716 ± 2	−448 ± 29	−284 ± 7	−524 ± 34	−332 ± 8
KJC[e]	0.67	−711 ± 27	−454 ± 29	−266 ± 25	−536 ± 40	−314 ± 32
KJB[e]	0.49	−721 ± 21	−438 ± 12	−255 ± 26	−510 ± 20	−297 ± 31
KJA[e]	0.38	−306 ± 40	−190 ± 30	−108 ± 23	−521 ± 106	−295 ± 74
KJE[f]	1.14	−595	−372	−246	−526 ± 7	−348 ± 10
KJD[f]	0.81	−601	−375	−235	−526 ± 7	−331 ± 10
KJC[f]	0.67	−622	−388	−235	−526 ± 6	−319 ± 9
KJ[f]	0.24–5.9	−658	−409	−250	−522 ± 5	−319 ± 9
R1CPD[g]	—	−255 ± 2	−159 ± 1	−98 ± 1	−523 ± 5	−322 ± 4
R1CPF[g]	—	−260 ± 2	−158 ± 1	−93 ± 1	−510 ± 5	−300 ± 4

[a] Amari et al. (1994).
[b] Calculated isotopic composition of the G-component, assuming a solar isotopic composition N-component (see text).
[c] This work, ± 2σ.
[d] Average grain size of KJG grains analyzed in this work, weighted by the total number of Ba atoms detected.
[e] SIMS data of Zinner et al. (1991), from Zinner (personal communication) because the published paper contained no data table, ± 2σ.
[f] TIMS data of Prombo et al. (1993), ± 2σ.
[g] TIMS data of Ott and Begemann (1990a), ± 2σ.

connecting the G- and *N*-components of aggregates KJA through KJH from our data and that of Zinner et al. (1991).

Previous studies on size-separated fractions from Murchison have shown an isotopic composition dependent on average particle size (Amari et al., 1994) for fractions covering the range 0.38 to 1.86 μm (Zinner et al., 1991; Prombo et al., 1993), and this effect may account for the fact that the new data on KJG single SiC grains show less *s*-process enrichment than previous data on aggregates of smaller-sized SiC grains. Amari et al. (1994) found that presolar SiC grains from Murchison follow a log-normal size distribution. Thus, in Figure 5 are plotted δ-values vs. log particle size (as measured directly by scanning electron microscopy) for the individual grains we analyzed, for the average data for all grains we analyzed, and for the literature data on aggregates. A log-linear correlation line was fitted to the grain size separates of Zinner et al. (1991) and Prombo et al. (1993), excluding the smallest fraction, KJA, which is anomalous and may represent the limits of centrifugation in isolating grains. The average data for all the KJG grains we analyzed lies on or very close to the correlation line through the smaller grain size separates. The δ values for ^{135}Ba, ^{137}Ba and ^{138}Ba are within 3, 4 and 2 standard deviations of the line, respectively. However, the uncertainties for the average KJG spectra are based on counting statistics alone and, given the real spread in δ values among individual grains and the low number of grains analyzed, are clearly an underestimate of present uncertainties in mean δ value of mainstream KJG grains. The data sets plotted in Figure 5 were acquired by three different techniques, yet the agreement among them for aggregates is excellent and our results are consistent with the prior observation that smaller mainstream SiC grains show the most *s*-processing.

The wide grain-to-grain variability evident in the single grain data shows that each grain is unique and retains the nucleosynthetic signature of its astrophysical site of origin. Size fraction

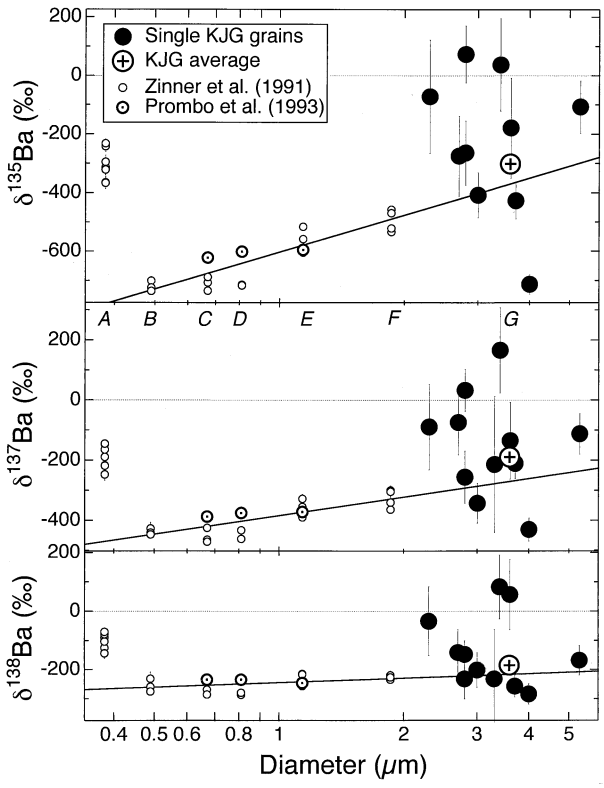

Fig. 5. Barium isotopic composition vs. log grain diameter for individual presolar grains, the average of the individual grains, and aggregate samples of grain-size separates from previous studies. The data of Zinner et al. (1991) were determined by SIMS; the remaining literature data on aggregates were determined by TIMS. A regression line is fitted through the aggregate grain-size separates, excluding the KJA value of Zinner et al. (1991). Note that the KJG average, derived from the total counts of all single grain spectra, which was not included in the regression, lies close to the regression line.

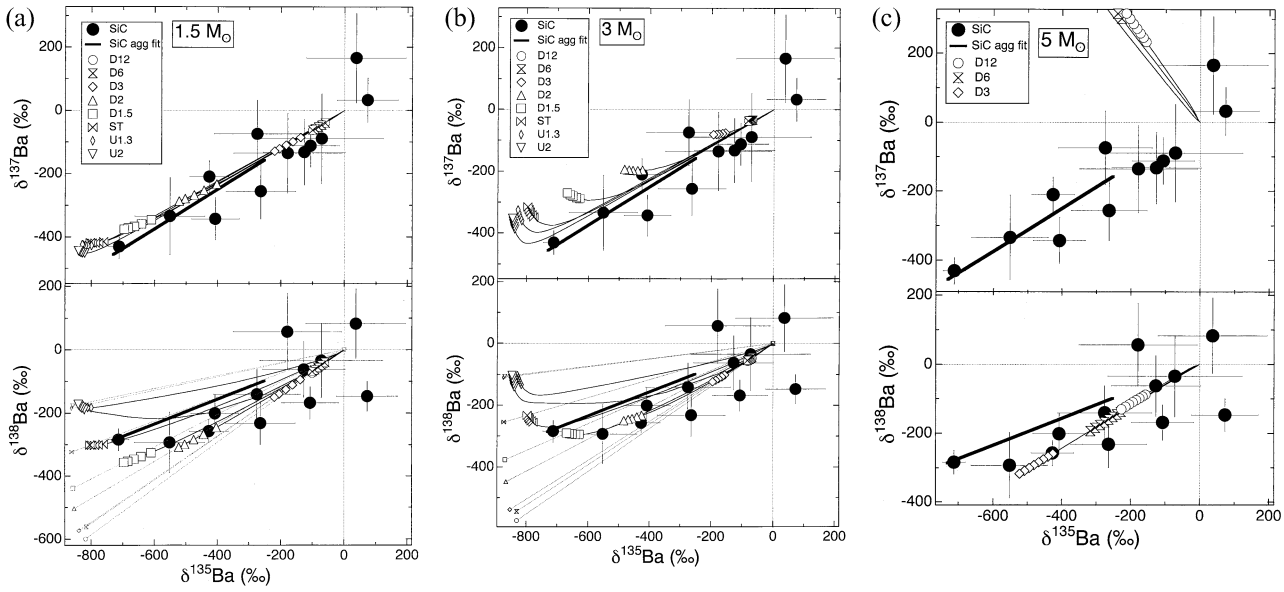

Fig. 6. δ^{137}Ba and δ^{138}Ba vs. δ^{135}Ba, comparing single presolar grain data and predictions for (a) 1.5, (b) 3, and (c) 5 $M_\odot$ AGB stars. Each point corresponds to the envelope composition after third dredge-up following each thermal pulse; points are plotted only for pulses for which the envelope C/O > 1. The heavy straight line in each panel represents the range of isotopic compositions previously measured in aggregate KJ by Prombo et al. (1993) (see Fig. 3). In the bottom panels of (a) and (b), the *N*- and G-components are plotted with small symbols for each ^{13}C pocket size and connected with dashed lines.

KJG represents only ~4% of the SiC in the KJ separate from the Murchison meteorite. We are currently improving our instrument and method to enable us to analyze smaller grains (Veryovkin et al., 2001; Savina et al., 2003). This will extend the data over a wider range and allow us to sample much smaller grains. It is clear that there is much grain-to-grain variation in barium isotopic composition among the large grains, and it remains to be seen if the same is true of the smaller grains that constitute the majority of the presolar SiC in the meteorite.

4. DISCUSSION

We begin by discussing nucleosynthesis of barium in AGB stars and then compare the barium isotopic compositions of single mainstream presolar SiC grains with model predictions.

4.1. *s*-Process Nucleosynthesis in AGB Stars

In the last few years, detailed studies of *s*-process nucleosynthesis in AGB stars have been performed by Gallino et al. (1997, 1998), Busso et al. (1999, 2001), Goriely and Mowlavi (2000), and Lugaro et al. (2003). According to these studies, the *s*-process in AGB stars is driven by two neutron sources: ^{13}C(α,n)^{16}O, activated during the interpulse period; and ^{22}Ne(α,n)^{25}Mg, activated during the thermal pulse. At the end of each third dredge-up episode, some hydrogen is assumed to be ingested into the top layers of the helium intershell. When the helium intershell contracts after the thermal pulse and hydrogen reignites at the base of the convective envelope, this hydrogen reacts with the abundant ^{12}C, via ^{12}C(p,γ)^{13}N($\beta^+\nu$)^{13}C, to enrich this region in ^{13}C, making a so-called ^{13}C pocket. All of this ^{13}C burns in radiative conditions in the interpulse period, via ^{13}C(α,n)^{16}O, releasing a large time-integrated neutron flux with relatively low neutron densities (in the range of 10^6 to 10^7 cm^{-3}, depending on the efficiency of the ^{13}C pocket). The amount of hydrogen ingested and its distribution within the helium intershell, which determines the amount and profile of the ^{13}C pocket, depends on hydrodynamic effects that are not well understood, so these are relatively free parameters in AGB models (see discussion in Busso et al., 1999). In the calculations presented here, the ^{13}C profile of Gallino et al. (1998) was used and only the amount of ^{13}C was varied. Note that the extent in radial mass fraction of the ^{13}C pocket, where proton diffusion was assumed to occur, is kept constant in all cases, ~1/20 of the helium intershell mass. As shorthand, we refer to this variable as ^{13}C pocket amount. The ^{22}Ne is produced in the thermal pulse by the chain ^{14}N(α,γ)^{18}F($\beta^+\nu$)^{18}O(α,γ)^{22}Ne, where ^{14}N results from hydrogen-burning ashes by the operation of the CNO cycle in the hydrogen-burning shell. The second neutron source, the ^{22}Ne(α,n)^{25}Mg reaction, is marginally activated in the pulse-driven convective zone near its maximum extension when the bottom temperature briefly reaches 3×10^8 K, producing a small time-integrated neutron flux with high neutron density (up to several 10^9 cm^{-3}). The duration of the neutron burst is only ~6 yr and the corresponding total neutron exposure is low. However, the ^{22}Ne neutron source can significantly affect the abundances of nuclides sensitive to branchings along the *s*-path.

A series of *s*-process models for solar metallicity AGB stars of 1.5, 3, and 5 $M_\odot$ were calculated for a variety of ^{13}C pocket amounts. The predictions of these models for the barium isotopes are plotted in Figures 6 and 7. Each model assumes initially solar isotopic and elemental composition. As ^{12}C and *s*-process isotopes are dredged up after thermal pulses, the C/O

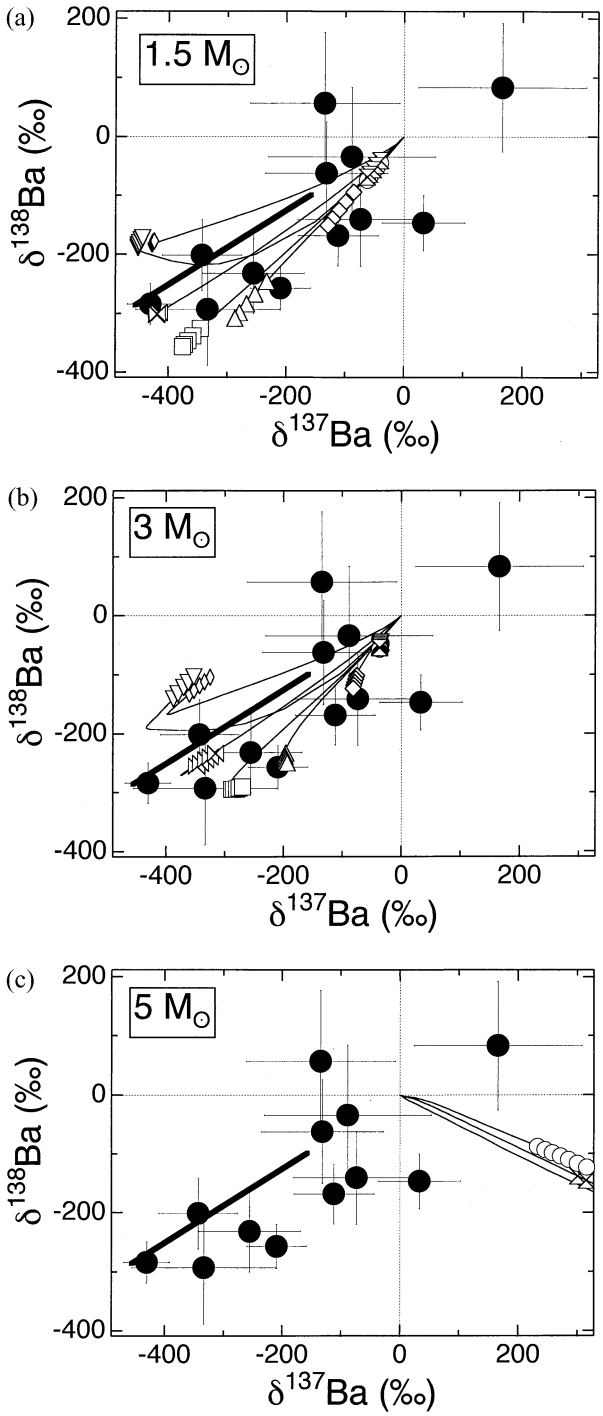

Fig. 7. δ^{138}Ba vs. δ^{137}Ba, comparing single presolar grain data with predictions for (a) 1.5 and (b) 3 $M_\odot$ AGB stars. Each point corresponds to the envelope composition after third dredge-up following each thermal pulse; points are plotted only for pulses for which the envelope C/O $>$ 1. The heavy straight line in each panel represents the range of isotopic compositions previously measured in aggregate KJ by Prombo et al. (1993) (see Fig. 4). See Figure 6 for legend.

ratio and the proportion of s-process isotopes in the envelope increases. In Figures 6 and 7, each case starts with a solar isotopic composition and evolves along a line. Progressive departure from the initial isotopic composition is due to progressive addition of *s*-process material from the helium intershell by TDU episodes. Loss of the envelope by stellar winds and from erosion by the advancing hydrogen-burning shell is accounted for in the calculation. TDU is obtained self-consistently in the FRANEC models used in this work (Straniero et al., 1997), but it may depend on the specific choice of the mass loss rate and of different algorithms for the treatment of the border between the radiative and convective zone. Symbols are plotted on the AGB envelope compositional evolution line only for those pulses for which the envelope has C/O $>$ 1. For AGB stars of initial mass 1.5 and 3 $M_\odot$, the standard case (ST) corresponds to the choice of the ^{13}C pocket amount and profile adopted by Gallino et al. (1998), which has been proven to reproduce the main component solar abundances of low mass AGB stars of one half solar metallicity (see also Arlandini et al., 1999). A total range of a factor of 24 in ^{13}C pocket amount was explored, from one-twelfth the ST case (D12), to twice the ST case (U2). The D12 case corresponds to essentially no hydrogen ingestion after thermal pulses to make ^{13}C; U2 corresponds to the maximum plausible ^{13}C pocket amount. Indeed, higher proton abundances penetrating into the top layers of the helium intershell during TDU would not result in a higher production of ^{13}C nuclei, because of the concurrent effect of proton captures on previously formed ^{13}C to make ^{14}N. Also, when ^{13}C nuclei later release neutrons via the reaction ^{13}C(α,n)^{16}O, the ^{14}N acts as a strong neutron poison, thus decreasing the effective ^{13}C neutron exposure.

Because metallicity and ^{13}C pocket efficiency are approximately complementary (since the ratio of the ^{13}C pocket amount to the metallicity determines the number of neutrons per seed nucleus for the *s*-process, neglecting in first order the effect of the ^{22}Ne neutron source), a similar isotopic distribution can be obtained by scaling the metallicity and ^{13}C pocket amount by the complementary factors. For example, the *s*-process isotope distribution obtained using the ST case in an AGB model of one half solar metallicity is almost the same as that obtained by a model with solar metallicity and U2 case. The range of ^{13}C pocket amounts adopted in this study has been demonstrated by Busso et al. (2001) and Abia et al. (2001, 2002) to cover the range of *s*-element abundances observed in chemically peculiar AGB stars and their descendants. It should be clear that the solar system *s*-process abundance distribution is in reality the outcome of all previous generations of AGB stars of varying masses and metallicities lower than solar, each of them producing a different *s*-process distribution of abundances (see discussion in Busso et al., 1999). For 5 $M_\odot$ stars, the helium intershell and TDU efficiency are an order of magnitude smaller than in 1.5 and 3 $M_\odot$ stars, so only the D12, D6 and D3 cases are plausible, and the mass dredged up after each thermal pulse is an order of magnitude lower (Lugaro et al., 2002). The ^{22}Ne source is more efficient here, since the maximum temperature in the bottom of the pulse-driven convective zone reaches 3.2 $\times$ 10^8 K. Consequently, effects on branching-dependent nuclei are more pronounced.

4.2. *s*-Process Nucleosynthesis of Barium

With regard to the *p*-process isotopes, we have calculated, but not plotted, δ^{130}Ba and δ^{132}Ba, because the abundances of

^{130}Ba and ^{132}Ba were too low to measure in single SiC grains. The calculations predict a variation in δ^{130}Ba and δ^{132}Ba from 0 to nearly −1000‰, reflecting the progressive mixing of the G-component with the *N*-component. As shown in Figure 1, ^{130}Ba and ^{132}Ba are bypassed by the *s*-process path, but their high neutron capture cross sections (Bao et al., 2000) dictate that their initial abundances are fully destroyed by the *s*-process in the helium intershell. The mass fractions of ^{130}Ba and ^{132}Ba remain essentially constant in the envelope of an AGB star, with only ~2% loss of their initial abundances at the last TDU episode, maintaining a memory of the initial *N*-component composition, whereas the fraction of ^{136}Ba and other *s*-process isotopes increase with successive third dredge-up episodes.

δ^{135}Ba is linear with δ^{130}Ba and δ^{132}Ba, but the calculated G-component has δ^{135}Ba of −846‰, not −1000‰, because a small amount of ^{135}Ba is produced in the *s*-process. This value is in good agreement with the value of −839‰ inferred by Prombo et al. (1993) from measurements of the Murchison KJ fraction, the parent for the KJA to KJH grain size separates of Amari et al. (1994).

There are a number of branchings in the *s*-process path (Fig. 1) that can be affected by the two neutron sources in AGB stars. Although ^{134}Ba and ^{136}Ba are both *s*-only, their predicted ratio shows a spread of values induced by the branch point at ^{134}Cs. This unstable nucleus has a half-life that is very sensitive to temperature: the laboratory half-life is 2.06 a, while at 1×10^8 K (typical of the ^{13}C neutron source) it decreases to 0.67 a. For this work, the half-life at 3×10^8 K (typical of the ^{22}Ne source) was calculated as 33 d by averaging the β-decay rates computed at selected temperatures and electron density values by Takahashi and Yokoi (1987) over the convective pulse. In fact, during a thermal pulse, a very large gradient in temperature and density exists, from $T \sim 3 \times 10^8$ K, $\rho = 2 \times 10^4$ g cm^{-3} in the bottom layers where most of the exposure occurs, to $T \sim 1 \times 10^7$ K, $\rho = 10$ g cm^{-3} in the top layers. Whereas neutrons are produced and captured locally in the various layers, the convective overturn time in the convection zone is less than one hour (Gallino et al., 1988; Käppeler et al., 1990; Wisshak et al., 2001). In the ^{13}C pocket, ^{134}Ba is more strongly produced than ^{136}Ba (relative to solar), because the low neutron density makes the β-decay channel at the ^{134}Cs branch point dominant. During the thermal pulse, the neutron capture channel at ^{134}Cs is substantially activated, despite the higher β-decay rate of ^{134}Cs, thus ^{134}Ba and ^{135}Ba are partly bypassed. The abundance of ^{134}Ba in the helium intershell at the quenching of the thermal pulse depends on the temperature at the bottom of the convective intershell, which varies from pulse to pulse and is sensitive to stellar mass.

The branch point at ^{134}Cs affects other isotopes, in particular the production of ^{135}Ba. The neutron capture channel at ^{134}Cs feeds ^{135}Cs, which is a long-lived nucleus ($T_{1/2} = 2$ Ma). Since ^{135}Cs accumulates during the *s*-process, ^{134}Ba and ^{135}Ba are bypassed during the thermal pulse. In the model predictions, ^{135}Cs decays to ^{135}Ba in the helium intershell and the envelope, but no ^{135}Cs was allowed to decay after SiC grain formation, because cesium is a volatile element and is not expected to condense into SiC grains. Lugaro et al. (2003) point out that such AGB models show excellent agreement with the aggregate data of Prombo et al. (1993) on a plot of δ^{135}Ba vs. δ^{130}Ba. If ^{135}Cs were allowed to decay completely before barium was incorporated into SiC, the predicted G-component would be ~100‰ higher in δ^{135}Ba. Although the Maxwellian average neutron capture cross sections of ^{134}Ba, ^{135}Ba, ^{136}Ba, and ^{137}Ba have recently been determined with an uncertainty of 3% at 30 keV (Bao et al., 2000), the situation concerning the neutron capture cross sections for unstable cesium isotopes is much less satisfactory. An experimental determination has been obtained for ^{135}Cs, with a 10% uncertainty, whereas for the other unstable cesium isotopes only theoretical estimates exist with estimated uncertainties of 30–50%. Also, the β-decay rate of ^{134}Cs at stellar temperatures is rather uncertain (Takahashi and Yokoi, 1987). However, using the recommended Bao et al. (2000) cross sections and the stellar β-decay rate of ^{134}Cs averaged over the convective pulse, Arlandini et al. (1999) were able to reproduce the solar ^{134}Ba/^{136}Ba ratio rather well for an AGB model that best reproduces the main *s*-process component of the solar system. The same was true for the prediction of this ratio by the chemical evolution of the Galaxy considering the contributions of all previous generations of AGB stars preceding the formation of the solar system (Travaglio et al., 1999), indicating that the differences between estimated and true values of the β-decay rate of ^{134}Cs and of its neutron capture cross section most likely compensate. Concerning single presolar SiC grains, much more precise measurements of barium isotope ratios in a larger number of grains are needed to better constrain the effects of the branchings involved. An important conclusion has already been reached with respect to the measurement of the ^{134}Ba/^{136}Ba ratio in aggregates of many grains, in which the ratio of these two *s*-process isotopes was found to be nonsolar (Ott and Begemann, 1990a; Zinner et al., 1991; Prombo et al., 1993): such nonsolar ratios can be matched by the present AGB model predictions of low mass stars of solar metallicity (Gallino et al., 1997; Lugaro et al., 2002).

The neutron capture channel at ^{135}Cs produces short-lived ^{136}Cs ($T_{1/2} = 13$ d), which decays to ^{136}Ba. However, during the peak neutron density from the ^{22}Ne neutron source, a small branch feeds the neutron magic unstable ^{137}Cs ($T_{1/2} = 30$ a). This nucleus has a low neutron capture cross section and accumulates during the thermal pulse. It decays to ^{137}Ba during the subsequent interpulse phase. The ^{22}Ne source is of relatively increasing importance with increasing stellar mass, because of progressively higher temperatures during late thermal pulses. On the plot of δ^{137}Ba vs. δ^{135}Ba (Fig. 6), the predicted curves are fairly straight for 1.5 $M_\odot$ (Fig. 6a), where the β-decay channel dominates at the ^{136}Cs branch; they bend upwards at the end for 3 $M_\odot$ (Fig. 6b), because of some activation of the neutron capture channel of the ^{136}Cs branch; and the curves have a negative slope for 5 $M_\odot$ (Fig. 6c), because of the dominance of the neutron capture channel of the ^{136}Cs branch during the later pulses when the envelope is carbon-rich. The major uncertainties in AGB model predictions for barium isotopes come from uncertainties in neutron capture cross sections for the unstable cesium isotopes, all of which are based on theoretical estimates. Additional uncertainties arise from calculated β^- decay rates.

Finally, we discuss ^{138}Ba. As already discussed in the Introduction, the ^{138}Ba/^{136}Ba ratio depends almost entirely on the major neutron exposure provided by the ^{13}C neutron source. This is to be expected, since ^{138}Ba is a neutron magic nucleus and consequently has a very low neutron capture cross section.

It therefore acts as a bottleneck in the *s*-process path and its abundance increases only slightly during a thermal pulse. As the ^{13}C pocket amount increases, the final δ^{138}Ba in the envelope varies significantly, first dropping from 0 to −300 to −350‰, then rising to −100 to −175‰ (Figs. 6 and 7). The model curves for each ^{13}C pocket amount bend upwards for the last thermal pulses, due to changes in the composition of the G-component. To emphasize this point, we have plotted in Figures 6a and b lines connecting the G- and *N*-components for the last pulse for each ^{13}C pocket amount. These changes reflect the fact that the *s*-process distribution (in particular the ratio of neutron magic ^{138}Ba to *s*-only ^{136}Ba) changes with the efficiency of the ^{13}C pocket (mean neutron exposure) as shown in the bottom panels of Figures 6a and b. Even with a given choice of ^{13}C pocket amount, the *s*-process distribution changes with thermal pulse number. The effect is related to both the increased contribution of the ^{22}Ne source and to the structural variations of subsequent thermal instabilities, in particular to the progressive decrease of the helium intershell mass (see Straniero et al., 1997). The G-component in the envelope must be considered to be the astrated helium shell material cumulatively mixed with the envelope by all previous third dredge-up episodes, diminished by the fraction lost in winds.

4.3. Comparison of SIC Grains with AGB Model Predictions

In prior studies of barium isotopes in presolar grain aggregates (Ott and Begemann, 1990a; Zinner et al., 1991; Prombo et al., 1993), the *N*-component was assumed to represent the initial compositions of AGB stars, but contamination of aggregates with solar system material was considered a possibility. Comparisons of aggregate and single-grain measurements with predictions on δ^{138}Ba vs. δ^{135}Ba plots (Fig. 6) are particularly revealing. The isotopic composition in the envelope after each TDU episode is indicated with a large symbol when C>O. From Figures 6 and 7, it can be seen that predictions for AGB stellar envelopes lie along curves, due to the changing isotopic composition of the G-component with progressive thermal pulses. We noted earlier that the single grain measurements tend to lie at lower δ^{138}Ba values than the aggregate correlation line on plots of δ^{138}Ba vs. δ^{135}Ba. Examination of Figure 6 shows that the lower δ^{138}Ba of the single grain data are consistent with the model predictions for 1.5 and 3 $M_\odot$ AGB stars within analytical uncertainties, although we cannot rule out the possibility that the single grains have some level of contamination. The higher precision aggregate data lie along lines between model predictions and solar system barium isotopic composition. It is likely that the aggregates have suffered varying degrees of contamination with solar system barium. There are many potential causes for this, including: barium contamination of SiC during laboratory separation from bulk Murchison; the presence of barium-rich solar system phases (Amari et al., 1994), such as hibonite, into the aggregates; and introduction of barium into SiC grains during aqueous activity on the Murchison parent body.

The conclusion that the aggregates lie along a line between likely AGB envelope barium isotopic composition and solar system composition due to varying degrees of solar system contamination brings up the issue of whether the *N*-component, the initial isotopic composition of AGB stars, is really of solar barium isotopic composition. The fact that single SiC grains with small δ^{135}Ba values lie near solar isotopic composition suggests that the average *N*-component is of approximately solar composition, but, as might be expected, there is some scatter among the single grains. The AGB stellar models assume solar initial isotopic composition and it appears from the single grain data that there are no gross exceptions to this assumption. Strontium, zirconium and molybdenum isotopic data in single mainstream presolar SiC grains also suggest that the parent AGB stars had initially solar proportions of *p*-, *r*- and *s*-process isotopes (Nicolussi et al., 1997a, 1998a,b). A substantial improvement in analytical precision of barium isotopic measurement of single SiC grains will be needed to further resolve this issue.

As long as the *N*-component is of solar composition, the calculated G-component is insensitive to possible contamination of presolar SiC with solar system barium. The variation in the δ^{138}Ba of the G-component in the models parallels the variation in the δ^{138}Ba seen in grain aggregates (Table 1 and Figs. 3 and 4). This suggests that the population of stars sampled in the different grain size aggregates varies in a systematic manner such that stars characterized by smaller ^{13}C pocket amounts tend to grow larger SiC grains in their circumstellar envelopes. The reasons for this are not clear.

Despite the limited amount of data presently available, the large spread observed in the single-grain data on the 3-isotope plots is a strong indicator that mainstream presolar SiC grains derive from many distinct AGB stars. The stellar models predict that the envelopes of carbon-rich 5 $M_\odot$ AGB stars will have large positive δ^{137}Ba (from the β^- decay of ^{137}Cs, see section 4.2), which is not observed in grains within reasonable error limits (Fig. 6c). Similar comparisons of strontium, zirconium, and molybdenum data on individual SiC grains with AGB model predictions also show that 5 $M_\odot$ AGB stars produce isotopic compositions not seen in grains (Nicolussi et al., 1997a, 1998a,b; Davis et al., 1998; Lugaro et al., 2003). This is consistent with the fact that intermediate-mass stars are generally prevented from becoming carbon-rich because of hot bottom burning. Furthermore, recent calculations show that even if such stars do become carbon-rich, the ^{12}C/^{13}C ratio would lie far outside the range observed in mainstream grains (Frost et al., 1998). Because stars of less than ~1.5 $M_\odot$ do not experience third dredge-up (Straniero et al., 1997), and our data preclude stars of ≥5 $M_\odot$, the mass of the progenitor stars is limited to ~1.5 to ~3 $M_\odot$. The range of the isotopic compositions observed in single grains shows that the nuclides in the grains experienced a range of neutron exposures, consistent with the current interpretation of spectroscopic data on various classes of *s*-enhanced stars (Abia et al., 2001; Busso et al., 2001). Although the array of possible ^{13}C pocket amounts for AGB stars of any given stellar mass can produce a wide array of isotopic compositions, each ^{13}C pocket amount can only produce grains with a narrow range of isotopic composition. Thus, the mainstream SiC grains must come from stars with a variety of ^{13}C pocket amounts. Over a limited range of metallicities, there is also a rough equivalence of metallicity and ^{13}C pocket amount: decreasing metallicity by a factor of two has about the same effect as increasing the ^{13}C pocket amount by a factor of two, because both cause the neutron/seed ratio to

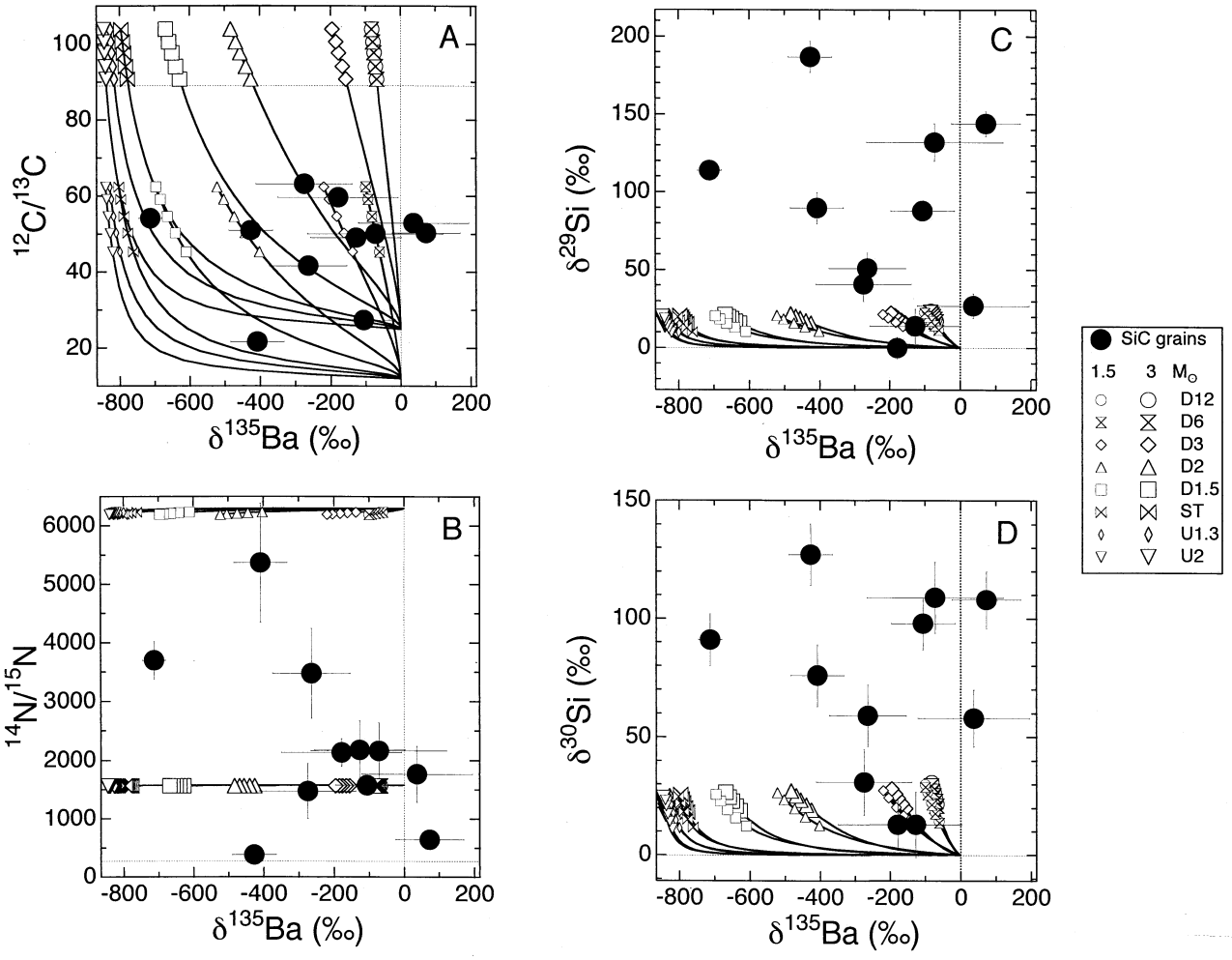

Fig. 8. Light element isotopic and barium isotopic compositions in single presolar SiC grain data compared with predictions for 1.5 and 3 $M_\odot$ AGB stars. The models assumed initially solar elemental and isotopic compositions. SiC grains with uncertainties larger than 300‰ for δ^{135}Ba are not plotted. Calculated points are plotted only for pulses for which the envelope C/O > 1. (a) $^{12}C/^{13}C$ vs. δ^{135}Ba; (b) $^{14}N/^{15}N$ vs. δ^{135}Ba; (c) δ^{29}Si vs. δ^{135}Ba; (d) δ^{30}Si vs. δ^{135}Ba.

increase by a factor of two. At one-third solar metallicity and below, this equivalence goes away, because of the increasing importance of the ^{22}Ne source.

Comparison of the barium data with zirconium and molybdenum data reveals a remaining puzzle. Zirconium and molybdenum measurements imply that most grains have more than 50% G-component, corresponding to $\delta^{96}Zr/^{94}Zr$ and $\delta^{92}Mo/^{96}Mo$ of less than −500‰ (Nicolussi et al., 1997a, 1998a; Davis et al., 1998). In contrast, only four of the twelve grains plotted in this study have more than 50% G-component, corresponding to a δ^{135}Ba value of less than about −400‰. AGB models clearly show that grains that have more than 50% G-component zirconium and molybdenum should also have more than 50% G-component barium. The discrepancy could be due to statistics, since relatively few grains were analyzed, but we note that strontium isotopic compositions of single SiC grains also show many grains with less than 50% G-component strontium (Nicolussi et al., 1998b). Strontium and barium may be somewhat more susceptible to contamination with solar system material, because strontium and barium elemental concentrations tend to show depletions relative to zirconium (Amari et al., 1995). It may also be that improvements in analytical techniques over the past few years (Savina et al., 2003) permit analysis of grains with lower trace element contents that might have been passed over in the earlier studies.

Most of the grains analyzed for barium isotopic composition also had their carbon, nitrogen, and silicon isotopic compositions measured. Single mainstream SiC grains are compared with predictions for 1.5 and 3 $M_\odot$ AGB stars on plots of $^{12}C/^{13}C$, $^{14}N/^{15}N$, δ^{29}Si and δ^{30}Si vs. δ^{135}Ba in Figure 8. There are no statistically significant correlations between any of the light element and barium isotopic compositions, except possibly for carbon. This is not surprising in the case of silicon, as silicon isotopes are not significantly affected by processes in solar metallicity AGB stars; Lugaro et al. (1999) suggest that silicon isotopes in mainstream grains may represent local heterogeneities in the interstellar medium at the time the parent stars of these grains were born combined with the general Galactic chemical trend, although Nittler (2002) argues that the interstellar medium was well-mixed and that

the silicon isotopic variations in mainstream grains reflect Galactic chemical evolution. Similarly, nitrogen isotopes are not affected by third dredge-up episodes in AGB star evolution. Nitrogen isotopes are modified in the envelope by first and second dredge-up (Huss et al., 1997), but these earlier stages do not affect barium isotopes. Nitrogen isotopes are significantly modified by the extramixing processes inferred to have modified carbon isotopes in carbon stars (see below). Extramixing before third dredge-up is a plausible explanation of the range in nitrogen isotopic composition in mainstream grains.

Carbon isotopic compositions of the envelopes of AGB stars are modified substantially during the thermal pulsing stage, as ^{12}C from helium-burning is mixed into the envelope with each third dredge-up episode. The $^{12}C/^{13}C$ ratio at the surface of a low mass AGB star of initially solar metallicity is assumed to be 89 at the end of the star's main sequence lifetime, but it must be different deep within the stellar envelope. Observations of carbon stars indicate that the assumption of an initial solar $^{12}C/^{13}C$ ratio is reasonable (Wallerstein and Knapp, 1998). As the star ascends the red giant branch, first dredge-up lowers the $^{12}C/^{13}C$ ratio at the surface to a canonical value of 20–30 and subsequent extramixing processes may further reduce this value (Charbonnel, 1994; Wasserburg et al., 1995). The extramixing process, which may occur in red giant stars with masses less than $\sim$2.5 $M_\odot$, lowers the $^{12}C/^{13}C$ ratio further. Compelling evidence for extramixing comes from spectroscopic observations of red giant stars (Gilroy, 1989; Gilroy and Brown, 1991). Thus, the envelopes of 1.5 and 3 $M_\odot$ stars have been taken in our models to have $^{12}C/^{13}C$ ratios of 12 and 25 respectively before the first thermal pulse with third dredge up (Fig. 8). The distribution of single mainstream grains on Figure 8a suggests that most come from stars with mass less than $\sim$2.5 $M_\odot$; none of the grains analyzed had $^{12}C/^{13}C$ in the higher range expected for 3 $M_\odot$ AGB stars. Two grains lie below the range expected for 1.5 $M_\odot$ AGB stars, which might imply a more efficient extramixing process. Examination of carbon isotopic analyses of all mainstream grains analyzed to date (see Lugaro et al., 1999, for a recent plot of $^{14}N/^{15}N$ vs. $^{12}C/^{13}C$) shows that most mainstream grains have $^{12}C/^{13}C > 40$. The two grains we analyzed with lower $^{12}C/^{13}C$ trend in the direction of A and B grains (which have $^{12}C/^{13}C < 10$) and their origins may be related. For a discussion of A and B grains, see Amari et al. (2001).

5. SUMMARY

Comparison of barium isotopic compositions of single mainstream presolar SiC grains with predictions for *s*-process nucleosynthesis in AGB stars shows that the grains come from AGB stars of 1.5 to perhaps 3 $M_\odot$ with initially solar proportions of *r*- and *s*-process isotopes and a wide variety of ^{13}C pocket sizes. The average composition of the grains studied here agrees with earlier results on grain aggregates that show that smaller grains tend to be more enriched in *s*-process isotopes than larger ones. Our data and that of Zinner et al. (1991) suggest that stars characterized by smaller ^{13}C pocket size tend to produce larger diameter SiC grains. The predicted isotopic signatures of stars of 5 $M_\odot$ are not seen in any grain, and support observations that the most massive progenitors of carbon stars do not exceed 3–5 $M_\odot$. Carbon isotopic compositions suggest that the upper mass limit of the parent AGB stars of mainstream SiC grains may be further restricted to $\sim$2.5 $M_\odot$.

Acknowledgments—This paper was originally presented orally at a symposium honoring the career of Robert N. Clayton in June 2001 and is dedicated to him. We thank Associate Editor Ulrich Ott for an extraordinarily careful review, and two anonymous reviewers and Marcel Arnould for their helpful comments. This work was supported by the Department of Energy, BES-Material Sciences through Contract No. W-31-109-ENG-38, by the National Aeronautics and Space Administration through grants 4493 (RNC), 8336 (SA), 9510 (AMD), and an unnumbered grant to MJP; by the University of Chicago, and by the Italian COFIN 2000 Progetto Osservabili Stellari di Interesse Cosmologico. Work supported by the U.S. Department of Energy, BES-Materials Sciences, under contract W-31-109-ENG-38 and NASA grants NAG5-4493, 8336, and 9510.

Associate editor: F. Podosek

REFERENCES

Abia C., Busso M., Gallino R., Domínguez I., Straniero O., and Isern J. (2001) The ^{85}Kr *s*-process branching and the mass of carbon stars. *Astrophys. J.* **559,** 1117–1134.

Abia C., Domínguez I., Gallino R., Busso M., Masera S., Straniero O., de Laverny P., Plez B., and Isern J. (2002) *s*-Process nucleosynthesis in carbon stars. *Astrophys. J.* **579,** 817–831.

Alaerts L., Lewis R. S., Matsuda J., and Anders E. (1980) Isotopic anomalies of noble gases in meteorites and their origins. VI. Presolar components in the Murchison C2 chondrite. *Geochim. Cosmochim. Acta* **44,** 189–209.

Amari S., Anders E., Virag A., and Zinner E. (1990) Interstellar graphite in meteorites. *Nature* **345,** 238–240.

Amari S., Lewis R. S., and Anders E. (1994) Interstellar grains in meteorites: I. Isolation of SiC, graphite, and diamond; size distributions of SiC and graphite. *Geochim. Cosmochim. Acta* **58,** 459–470.

Amari S., Hoppe P., Zinner E., and Lewis R. S. (1995) Trace-element concentrations in single circumstellar silicon carbide grains from the Murchison meteorite. *Meteoritics* **30,** 679–693.

Amari S., Zinner E., and Lewis R. S. (1999) A singular presolar SiC grain with extreme ^{29}Si and ^{30}Si excesses. *Astrophys. J.* **517,** L59–L62.

Amari S., Nittler L. R., Zinner E., Lodders K., and Lewis R. S. (2001) Presolar SiC grains of type A, and B: Their isotopic compositions and stellar origins. *Astrophys. J.* **559,** 463–483.

Arlandini C., Käppeler F., Wisshak K., Gallino R., Lugaro M., Busso M., and Straniero O. (1999) Neutron capture in low-mass asymptotic giant branch stars: Cross sections and abundance signatures. *Astrophys. J.* **525,** 886–900.

Bao Z. Y., Beer H., Käppeler F., Voss F., Wisshak K., and Rauscher T. (2000) Neutron cross sections for nucleosynthesis studies. *At. Data Nucl. Data Tables.* **76,** 70–154.

Beer H., Voss F., and Winters R. R. (1992) On the calculation of Maxwellian-averaged capture cross sections. *Astrophys. J.* **80**(Suppl.), 403–424.

Bernatowicz T., Fraundorf G., Tang M., Anders E., Wopenka B., Zinner E., and Fraundorf P. (1987) Evidence for interstellar SiC in the Murray carbonaceous meteorite. *Nature* **330,** 728–730.

Boothroyd A. I., Sackmann I.-J., and Ahern S. C. (1993) Prevention of high-luminosity carbon stars by hot bottom burning. *Astrophys. J.* **416,** 762–768.

Burbidge E. M., Burbidge G. R., Fowler W. A., and Hoyle F. (1957) Synthesis of the elements in stars. *Rev. Mod. Phys.* **29,** 547–650.

Busso M., Gallino R., and Wasserburg G. J. (1999) Nucleosynthesis in asymptotic giant branch stars: Relevance for galactic enrichment and solar system formation. *Annu. Rev. Astron. Astrophys.* **37,** 239–309.

Busso M., Gallino R., Lambert D. L., Travaglio C., and Smith V. V. (2001) Nucleosynthesis and mixing on the asymptotic giant branch. III. Predicted and observed *s*-process abundances. *Astrophys. J.* **557,** 802–821.

Charbonnel C. (1994) Clues for non-standard mixing on the red giant branch from $^{12}C/^{13}C$ and $^{12}C/^{14}N$ ratios in evolved stars. *Astron. Astrophys.* **282,** 811–820.

Choi B.-G., Huss G. R., Wasserburg G. J., and Gallino R. (1998) Presolar corundum and spinel in ordinary chondrites: Origins from AGB stars and a supernova. *Science* **282,** 1284–1289.

Choi B.-G., Wasserburg G. J., and Huss G. R. (1999) Circumstellar hibonite and corundum and nucleosynthesis in asymptotic giant branch stars. *Astrophys. J.* **522,** L133–L136.

Clayton D. D. (1968) *Principles of Stellar Evolution and Nucleosynthesis.* McGraw-Hill.

Davis A. M., Nicolussi G. K., Pellin M. J., Lewis R. S., and Clayton R. N. (1998) Heavy element isotopic compositions of single circumstellar grains from meteorites: Direct measurement of nucleosynthesis products from individual stars. In *Nuclei in the Cosmos V* (eds. N. Prantzos and S. Harissopulos), pp. 563–566. Editions Frontières.

Davis A. M., Pellin M. J., Lewis R. S., Amari S., and Clayton R. N. (1999) Light and heavy element isotopic compositions of mainstream SiC grains (abstract). *Lunar Planet. Sci.* **30,** 1976.

Davis A. M., Lugaro M., Gallino R., Pellin M. J., Lewis R. S., and Clayton R. N. (2001) Isotopic compositions of heavy elements in presolar grains: New constraints on nucleosynthesis. *Mem. Soc. Astron. It.* **72,** 413–421.

Frost C. A. and Lattanzio J. C. (1996) On the numerical treatment and dependence of the third dredge-up phenomenon. *Astrophys. J.* **473,** 383–387.

Frost C. A., Cannon R. C., Lattanzio J. C., Wood P. R., and Forestini M. (1998) The brightest carbon stars. *Astron. Astrophys.* **332,** L17–L20.

Gallino R., Busso M., Picchio G., Raiteri C. M., and Renzini A. (1988) On the role of low-mass asymptotic giant branch stars in producing a solar system distribution of *s*-process isotopes. *Astrophys. J.* **334,** L45–L49.

Gallino R., Raiteri C. M., and Busso M. (1993) Carbon stars and isotopic Ba anomalies in meteoritic SiC grains. *Astrophys. J.* **410,** 400–411.

Gallino R., Busso M., and Lugaro M. (1997) Neutron capture nucleosynthesis in AGB stars. In *Astrophysical Implications of the Laboratory Study of Presolar Materials* (eds. T. J. Bernatowicz and E. Zinner), AIP Conference Proceedings, Vol. 402, pp. 115–153. AIP.

Gallino R., Arlandini C., Busso M., Lugaro M., Travaglio C., Straniero O., Chieffi A., and Limongi M. (1998) Evolution and nucleosynthesis in low-mass asymptotic giant branch stars. II. Neutron capture and the *s*-process. *Astrophys. J.* **497,** 388–403.

Gilroy K. K. (1989) Carbon isotope ratios and lithium abundances in open cluster giants. *Astrophys. J.* **347,** 835–848.

Gilroy K. K. and Brown J. A. (1991) Carbon isotope ratios along the giant branch of M67. *Astrophys. J.* **371,** 578–583.

Goriely S. and Mowlavi N. (2000) Neutron-capture nucleosynthesis in AGB stars. *Astron. Astrophys.* **362,** 599–614.

Herwig F. (2000) The evolution of AGB stars with convective overshoot. *Astron. Astrophys.* **360,** 952–968.

Hidaka H., Holliger P., and Masuda A. (1993) Evidence of fissiogenic Cs estimated from Ba isotopic deviations in an Oklo natural reactor zone. *Earth Planet. Sci. Lett.* **114,** 391–396.

Huss G. R., Hutcheon I. D., and Wasserburg G. J. (1997) Isotopic systematics of presolar silicon carbide from the Orgueil (CI) chondrite: Implications for solar system formation and stellar nucleosynthesis. *Geochim. Cosmochim. Acta* **61,** 5117–5148.

Hutcheon I. D., Huss G. R., Fahey A. J., and Wasserburg G. J. (1994) Extreme ^{26}Mg and ^{17}O enrichments in an Orgueil corundum: Identification of a presolar oxide grain. *Astrophys. J.* **425,** L97–L100.

Iben I. Jr. and Renzini A. (1983) Asymptotic giant branch evolution and beyond. *Annu. Rev. Astron. Astrophys.* **21,** 271–342.

Jennings C. L., Savina M. R., Messenger S., Amari S., Nichols R. H. Jr., Pellin M. J., and Podosek F. A. (2002) Indarch SiC by TIMS, RIMS, and NanoSIMS (abstract). *Lunar Planet. Sci.* **33,** 1833.

Käppeler F., Beer H., and Wisshak K. (1989) *s*-Process nucleosynthesis—Nuclear physics and the classical model. *Rep. Prog. Phys.* **52,** 945–1013.

Käppeler F., Gallino R., Busso M., Picchio G., and Raiteri C. M. (1990) *s*-Process nucleosynthesis: Classical approach and asymptotic giant branch models for low-mass stars. *Astrophys. J.* **354,** 630–643.

Koehler P. E., Spencer R. R., Guber K. H., Winters R. R., Raman S., Harvey J. A., Hill N. W., Blackmon J. C., Bardayan D. W., Larson D. C., Lewis T. A., Pierce D. E., and Smith M. S. (1998) High resolution neutron capture and transmission measurements on ^{137}Ba and their impact on the interpretation of meteoric barium anomalies. *Phys. Rev. C* **57,** 1558–1561.

Lattanzio J. C. and Boothroyd A. I. (1997) Nucleosynthesis of elements in low to intermediate mass stars through the AGB phase. In *Astrophysical Implications of the Laboratory Study of Presolar Materials* (eds. T. J. Bernatowicz and E. K. Zinner), AIP Conference Proceedings, Vol. 402, pp. 85–114. AIP.

Lewis R. S., Anders E., Shimamura T., and Lugmair G. W. (1983) Barium isotopes in Allende meteorite: Evidence against an extinct superheavy element. *Science* **222,** 1013–1015.

Lewis R. S., Tang M., Wacker J. F., Anders E., and Steel E. (1987) Interstellar diamonds in meteorites. *Nature* **326,** 160–162.

Lewis R. S., Amari S., and Anders E. (1990) Meteoritic silicon carbide: Pristine material from carbon stars. *Nature* **348,** 293–298.

Lewis R. S., Amari S., and Anders E. (1994) Interstellar grains in meteorites: II. SiC and its noble gases. *Geochim. Cosmochim. Acta* **58,** 471–494.

Lodders K. and Fegley B. Jr. (1995) The origin of circumstellar silicon carbide grains found in meteorites. *Meteoritics* **30,** 661–678.

Lugaro M., Zinner E., Gallino R., and Amari S. (1999) Si isotopic ratios in mainstream presolar SiC grains revisited. *Astrophys. J.* **527,** 369–394.

Lugaro M., Davis A. M., Gallino R., Pellin M. J., Straniero O., and Käppeler F. (2003) Isotopic compositions of strontium, zirconium, molybdenum, and barium in single presolar siC grains and asymptotic giant branch stars. *Astrophys. J.*, **593** (1), 486–508.

Ma Z., Thompson R. N., Lykke K. R., Pellin M. J., and Davis A. M. (1995) New instrument for microbeam analysis incorporating submicron imaging and resonance ionization mass spectrometry. *Rev. Sci. Instrum.* **66,** 3168–3176.

Messenger S., Keller L. P., and Walker R. M. (2002) Discovery of abundant interstellar silicates in cluster IDPs (abstract). *Lunar Planet. Sci.* **33,** 1887.

Mowlavi N. (1999) On the third dredge-up phenomenon in asymptotic giant branch stars. *Astron. Astrophys.* **344,** 617–631.

Nicolussi G. K., Davis A. M., Pellin M. J., Lewis R. S., Clayton R. N., and Amari S. (1997a) *s*-Process zirconium in presolar silicon carbide grains. *Science* **277,** 1281–1283.

Nicolussi G. K., Pellin M. J., Calaway W. F., Lewis R. S., Davis A. M., Amari S., and Clayton R. N. (1997b) Isotopic analysis of Ca from extraterrestrial micrometer-sized SiC by laser desorption and resonant ionization mass spectroscopy. *Anal. Chem.* **69,** 1140–1146.

Nicolussi G. K., Pellin M. J., Lewis R. S., Davis A. M., Amari S., and Clayton R. N. (1998a) Molybdenum isotopic composition of individual presolar silicon carbide grains from the Murchison meteorite. *Geochim. Cosmochim. Acta* **62,** 1093–1104.

Nicolussi G. K., Pellin M. J., Lewis R. S., Davis A. M., Clayton R. N., and Amari S. (1998b) Strontium isotopic composition in individual circumstellar silicon carbide grains: A record of *s*-process nucleosynthesis. *Phys. Rev. Lett.* **81,** 3583–3586.

Nittler L. R., Alexander C. M. O'D., Gao X., Walker R. M., and Zinner E. K. (1994) Interstellar oxide grains from the Tieschitz ordinary chondrite. *Nature* **370,** 443–446.

Nittler L. R., Hoppe P., Alexander C. M. O'D., Amari S., Eberhardt P., Gao X., Lewis R. S., Strebel R., Walker R. M., and Zinner E. (1995) Silicon nitride from supernovae. *Astrophys. J.* **453,** L25–L28.

Nittler L. R. (2002) Meteoritic stardust and the clumpiness of Galactic chemical evolution (abstract). *Lunar Planet. Sci.* **33,** 1650.

Olnon F. M., et al. (1986) IRAS catalogues and atlases. Atlas of low-resolution spectra. *Astron. Astrophys. Suppl. Ser.* **65,** 607–1065.

Ott U., Begemann F., Yang J., and Epstein S. (1988) *s*-Process krypton of variable isotopic composition in the Murchison meteorite. *Nature* **332,** 700–702.

Ott U. and Begemann F. (1990a) Discovery of *s*-process barium in the Murchison meteorite. *Astrophys. J.* **353,** L57–L60.

Ott U. and Begemann F. (1990b) *s*-Process material in Murchison: Sr and more on Ba (abstract). *Lunar Planet. Sci.* **21,** 920–921.

Pellin M. J., Davis A. M., Lewis R. S., Amari S., and Clayton R. N. (1999) Molybdenum isotopic composition of single silicon carbide grains from supernovae (abstract). *Lunar Planet. Sci.* **30,** 1969.

Pellin M. J., Calaway W. F., Davis A. M., Lewis R. S., Amari S., and Clayton R. N. (2000a) Toward complete isotopic analysis of individual presolar silicon carbide grains: C, N, Si, Sr, Zr, Mo, and Ba in single grains of Type X (abstract). *Lunar Planet. Sci.* **31,** 1917.

Pellin M. J., Davis A. M., Calaway W. F., Lewis R. S., Clayton R. N., and Amari S. (2000b) Zr and Mo isotopic constraints on the origins of unusual types of presolar SiC grains (abstract). *Lunar Planet. Sci.* **30,** 1934.

Pellin M. J., Davis A. M., Savina M. R., Kashiv Y., Clayton R. N., Lewis R. S., and Amari S. (2001) Barium isotopes in single presolar grains (abstract). *Lunar Planet. Sci.* **30,** 2125.

Prombo C. A., Podosek F. A., Amari S., and Lewis R. S. (1993) *s*-Process Ba isotopic compositions in presolar SiC from the Murchison meteorite. *Astrophys. J.* **410,** 393–399.

Richter S., Ott U., and Begemann F. (1992) *s*-Process isotope anomalies: Neodymium, samarium, and a bit more of strontium (abstract). *Lunar Planet. Sci.* **23,** 1147–1148.

Richter S., Ott U., and Begemann F. (1993) *s*-Process isotope abundance anomalies in meteoric silicon carbide: New data. In *Nuclei in the Cosmos II* (eds. F. Käppeler and K. Wisshak), pp. 127–132. Institute of Physics.

Richter S., Ott U., and Begemann F. (1994a) *s*-Process isotope abundance anomalies in meteoritic silicon carbide: Data for dysprosium. *Meteoritics* **29,** 522–523.

Richter S., Ott U., and Begemann F. (1994b) *s*-Process isotope abundance anomalies in meteoritic silicon carbide: Data for Dy. In *Proceedings of the European Workshop on Heavy Element Nucleosynthesis* (eds. E. Somorjai and Z. Fülöp), pp. 44–46. Institute of Nuclear Research of the Hungarian Academy of Science.

Savina M. R., Pellin M. J., Tripa C. E., Veryovkin I. V., Calaway W. F., and Davis A. M. (2003) Analyzing individual presolar grains with CHARISMA. *Geochim. Cosmochim. Acta*, this issue.

Schwarzschild M. and Härm R. (1965) Thermal instability in nondegenerate stars. *Astrophys. J.* **142,** 855–867.

Sharp C. M. and Wasserburg G. J. (1995) Molecular equilibria and condensation temperatures in carbon-rich gases. *Geochim. Cosmochim. Acta* **59,** 1633–1652.

Srinivasan B. and Anders E. (1978) Noble gases in the Murchison meteorite: Possible relics of *s*-process nucleosynthesis. *Science* **201,** 51–56.

Straniero O., Chieffi A., Limongi M., Busso M., Gallino R., and Arlandini C. (1997) Evolution and nucleosynthesis in low-mass asymptotic giant branch stars. I. Formation of population I carbon stars. *Astrophys. J.* **478,** 332–339.

Takahashi K. and Yokoi K. (1987) Beta-decay rates of highly ionized heavy atoms in stellar interiors. *At. Data Nucl. Data Tables* **36,** 375–409.

Tang M. and Anders E. (1988) Isotopic anomalies of Ne, Xe, and C in meteorites. II. Interstellar diamond and SiC: Carriers of exotic noble gases. *Geochim. Cosmochim. Acta* **52,** 1235–1244.

Travaglio C., Galli D., Gallino R., Busso M., Ferrini F., and Straniero O. (1999) Galactic chemical evolution of heavy elements from barium to europium. *Astrophys. J.* **521,** 691–702.

Treffers R. and Cohen M. (1974) High-resolution spectra of cool stars in the 10- and 20-micron regions. *Astrophys. J.* **188,** 545–552.

Veryovkin I. V., Calaway W. F., Moore J. F., King B. V., and Pellin M. J. (2001) An ultra-sensitive time-of-flight mass spectrometer for quantitative surface analysis. 14th Annual SIMS Workshop, Scottsdale, Ariz., pp. 53–55.

Volk K., Kwok S., Stencel R. E., and Brugel E. (1991) New low-resolution spectrometer spectra for IRAS sources. *Astrophys. J. Suppl. Ser.* **77,** 607–645.

Voss F., Wisshak K., Guber K., Käppeler F., and Reffo G. (1994) Stellar neutron capture cross sections of the Ba isotopes. *Phys. Rev. C Nucl. Phys.* **50,** 2582–2601.

Wallerstein G., Iben I. Jr., Parker P., Boesgaard A. M., Hale G. M., Champagne A. E., Barnes C. A., Käppeler F., Smith V. V., Hoffman R. D., Timmes F. X., Sneden C., Boyd R. N., Meyer B. S., and Lambert D. L. (1997) Synthesis of the elements in stars: Forty years of progress. *Rev. Mod. Phys.* **69,** 995–1084.

Wallerstein G. and Knapp G. R. (1998) Carbon stars. *Annu. Rev. Astron. Astrophys.* **36,** 369–433.

Wasserburg G. J., Boothroyd A. I., and Sackmann I.-J. (1995) Deep circulation in red giant stars: A solution to the carbon and oxygen isotope puzzles? *Astrophys. J.* **447,** L37–L40.

Wisshak K., Voss F., Arlandini C., Becvář F., Straniero O., Gallino R., Heil M., Käppeler F., Krticka M., Masera S., Reifarth R., and Travaglio C. (2001) Neutron capture on $^{180}Ta^{m}$: Clue for an s-process origin of nature's rarest isotope. *Phys. Rev. Lett.* **87,** 25110.2/1–251102/4.

Zinner E., Amari S., and Lewis R. S. (1991) s-Process Ba, Nd, and Sm in presolar SiC from the Murchison meteorite. *Astrophys. J.* **382,** L47–L50.

Zinner E. (1998) Stellar nucleosynthesis and the isotopic composition of presolar grains from primitive meteorites. *Annu. Rev. Earth Planet. Sci.* **26,** 147–188.